Supplementary Information

Highly efficient white-light emission and UV-visible/NIR luminescence sensing of lanthanide metal-organic frameworks

Xinyu Wang, Pengfei Yan, Yuxin Li, Guanghui An, Xu Yao and Guangming Li*

Key Laboratory of Functional Inorganic Material Chemistry (MOE), School of Chemistry and Materials Science, Heilongjiang University, No. 74, Xuefu Road, Nangang District, Harbin 150080, People's Republic of China

Characterization. The FT-IR spectra of complexes **1**–**10** exhibit similar patterns (Figure S1). In a typical spectrum of complex **1**, the broad band around 3471 cm^{-1} is attributed to the characteristic peak of O–H bonds from the solvent molecules in the complex. The asymmetric and symmetric stretching vibrations of carboxylate groups are observed at 1647, 1596, and 1393 cm^{-1}. The appearance of the characteristic band at 1647 cm^{-1} indicates the deprotonation of the carboxylate groups and coordination to the lanthanide ions. UV-vis absorption spectra of the H_4L and complexes **1**–**10** were conducted in methanol solution and exhibit a similar pattern (Figure S2). The main absorption bands at 217 nm is attributed to the π–π^* transitions of the benzene rings. TG analyses support that there are crystalline solvents in complexes **1**–**10** (Figure S3). For example, complex **1** exhibits a gradual weight loss of 1.3% in the temperature range of 30–180 °C, which corresponds to the loss of solvent molecules in complex **1** (calculated 1.5%). Other calculations for crystalline solvents in complexes **2**–**10** are shown in Figure S3. Powder X-ray diffraction (PXRD) analysis demonstrates that the crystal structures of complexes **1**–**10** are in agreement with the simulated patterns, clearly indicating that the pure phases were obtained (Figure S4).

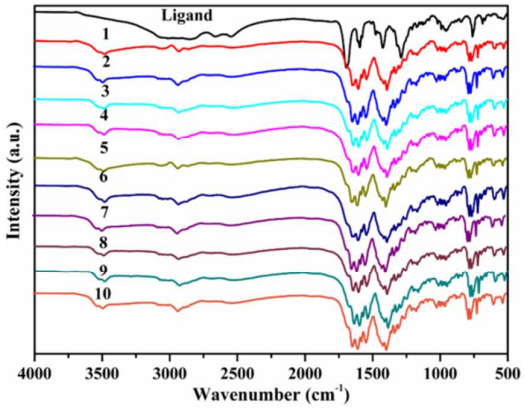

Figure S1. Infrared spectra of H_4L and complexes **1**–**10.**

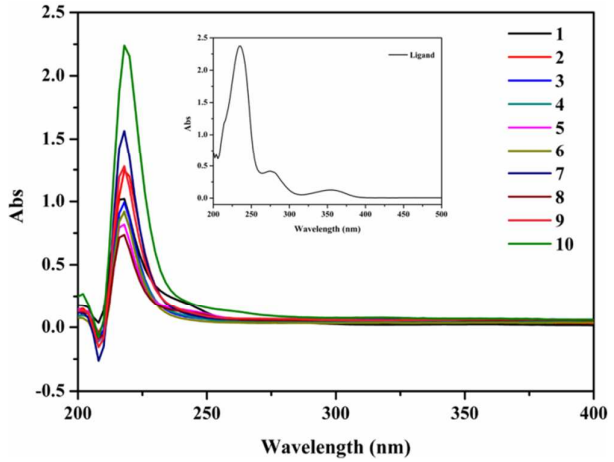

Figure S2. Ultraviolet spectra of H_4L and complexes **1**–**10.**

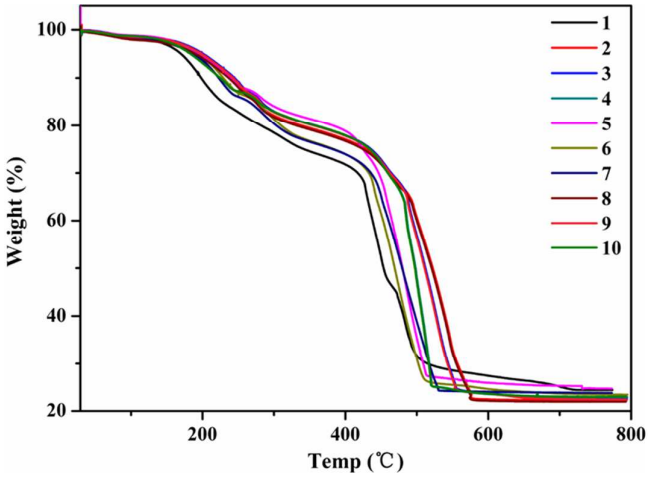

Figure S3. TG curves of complexes **1-10.**

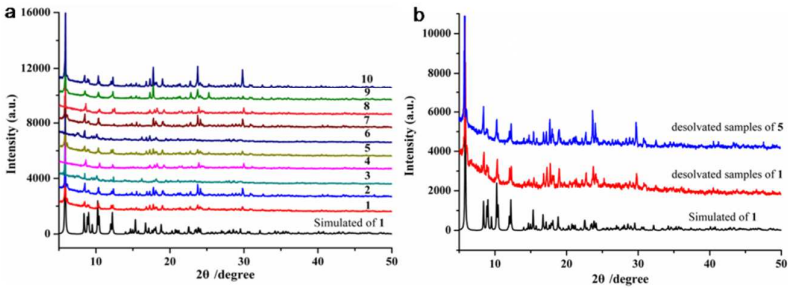

Figure S4. (a) PXRD patterns of complex **1** simulated from the X-ray single-crystal structure and as-synthesized samples of complexes **1-10**. (b) PXRD patterns of complex **1** simulated from the X-ray single-crystal structure and desolvated samples of complexes **1** and **5**.

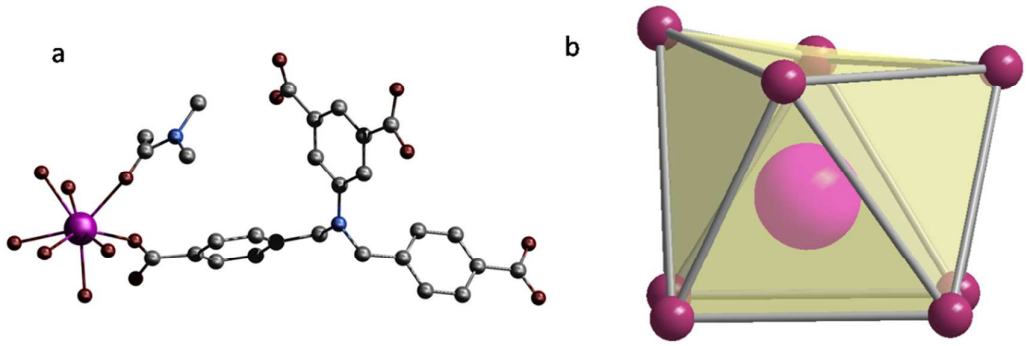

Figure S5. (a) The asymmetric unit of complex **5**. All hydrogen atoms and solvent molecules are omitted. (b) Coordination polyhedrons of Eu^{3+} ions.

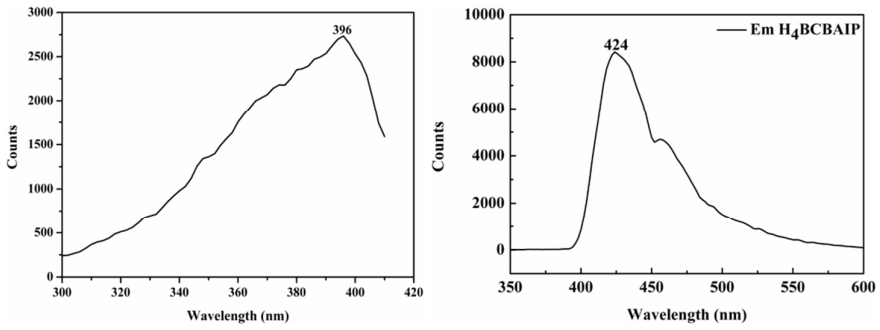

Figure S6. Solid state excitation (left) and emission (right) spectra of free H_4L ligand.

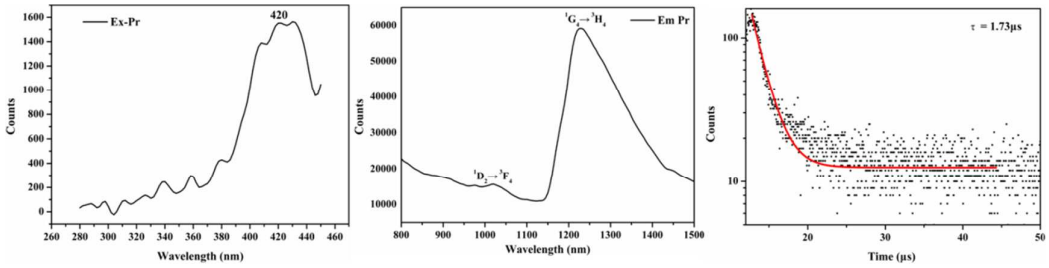

Figure S7 . Solid state excitation, emission spectra and Room-temperature luminescence decay curves of complex **2**.

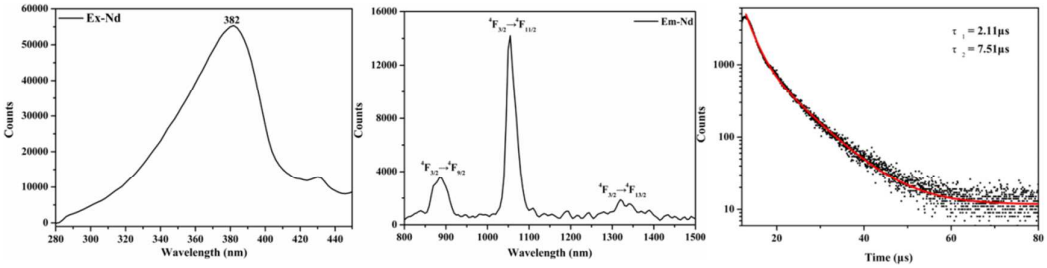

Figure S8. Solid state excitation, emission spectra and Room-temperature luminescence decay curves of complex **3**.

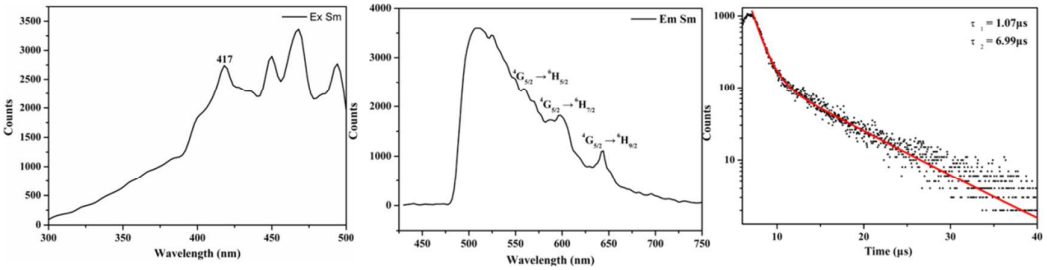

Figure S9. Solid state excitation, emission spectra and Room-temperature luminescence decay curves of complex **4**.

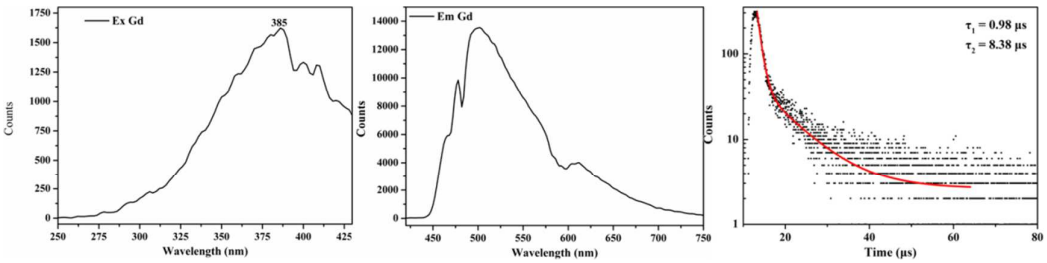

Figure S10. Solid state excitation, emission spectra and Room-temperature luminescence decay curves of complex **6**.

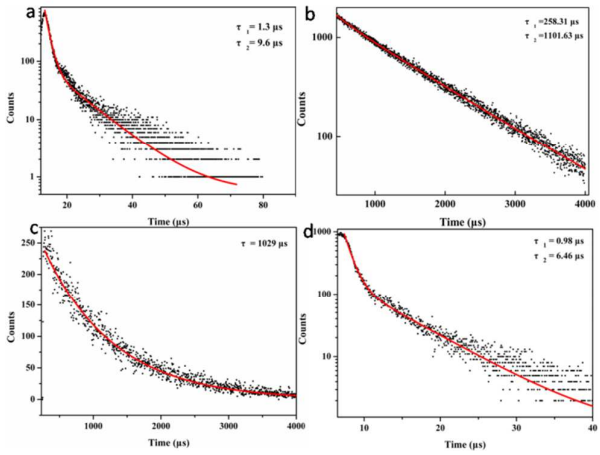

Figure S11. Room-temperature luminescence decay curves of complexes **1** (a), **5** (b), **7** (c) and **8** (d).

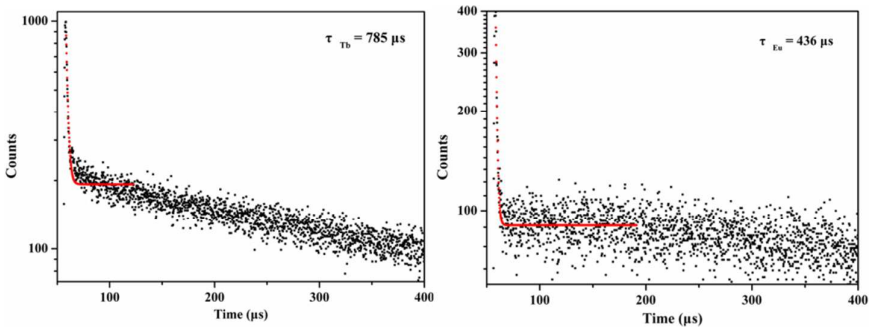

Figure S12. Room-temperature luminescence decay curves of complex **9** (monitored at 542 and 614 nm).

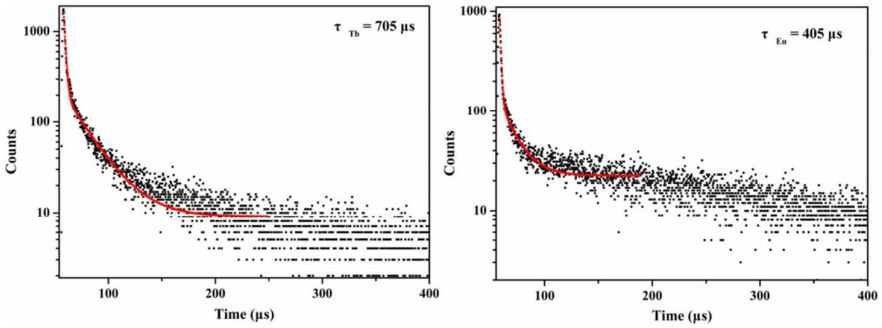

Figure S13. Room-temperature luminescence decay curves of complex **10** (monitored at 542 and 614 nm).

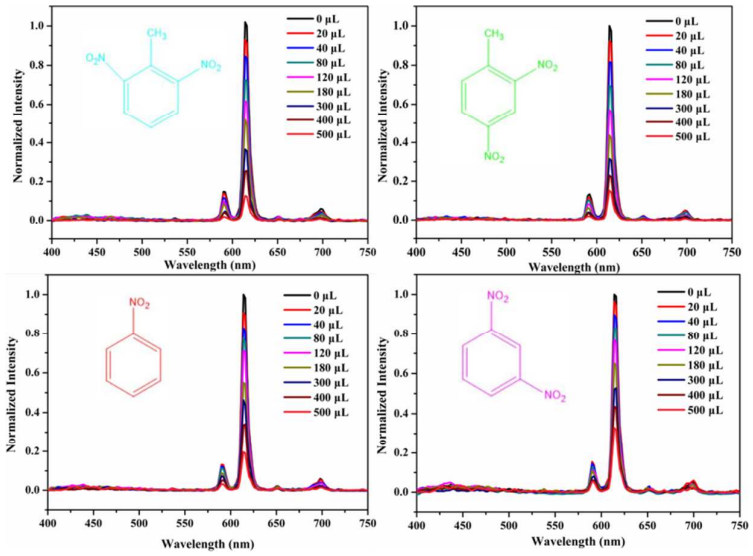

Figure S14. The fluorescence spectrum of complex **5** dispersed in DMAC with the addition of different content of nitro aromatic compounds at excitation 382 nm.

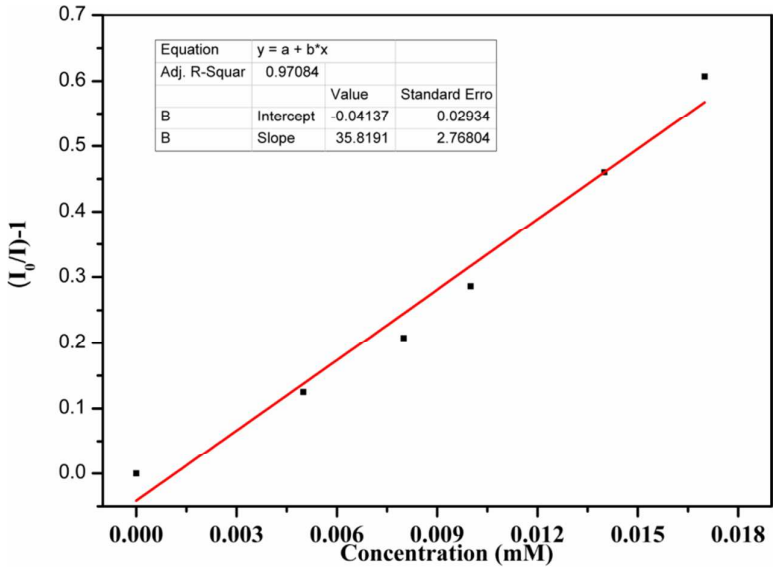

Figure S15. The Stern-Volmer plots for complex **5** with TNP in the low concentration region. The solid lines represent fits to the concertration-resolved data using the Stern-Volmer equation.

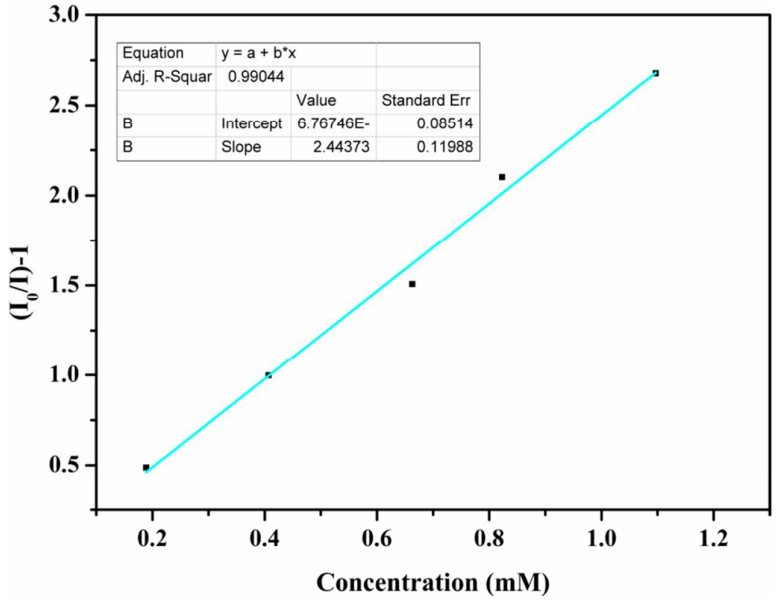

Figure S16. The Stern-Volmer plots for complex **5** with 2,6-DNT in the low concentration region. The solid lines represent fits to the concertration-resolved data using the Stern-Volmer equation.

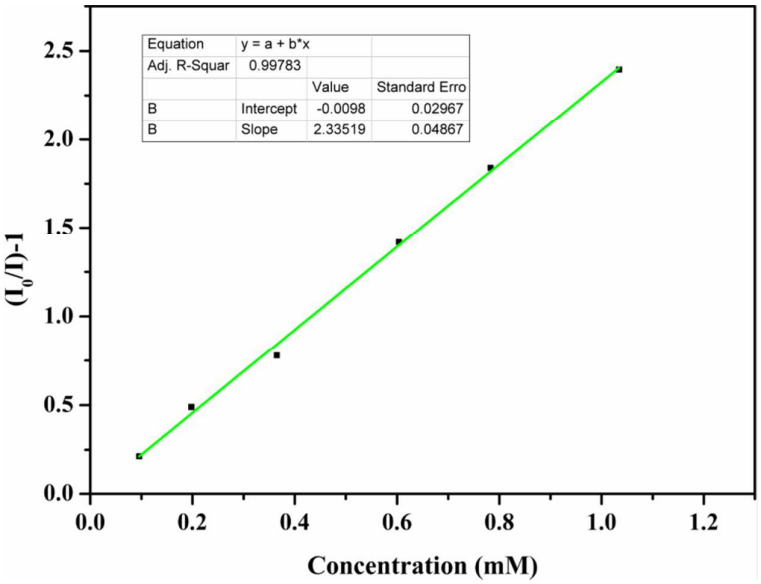

Figure S17. The Stern-Volmer plots for complex **5** with 2,4-DNT in the low concentration region. The solid lines represent fits to the concertration-resolved data using the Stern-Volmer equation.

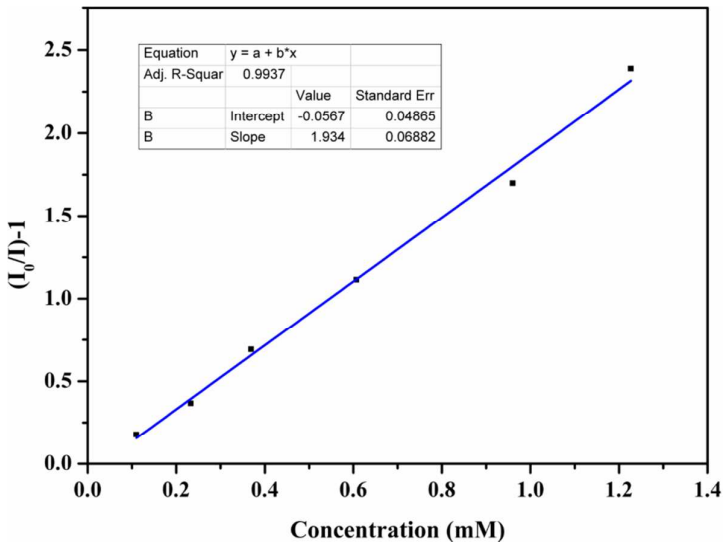

Figure S18. The Stern-Volmer plots for complex **5** with NB in the low concentration region. The solid lines represent fits to the concertration-resolved data using the Stern-Volmer equation.

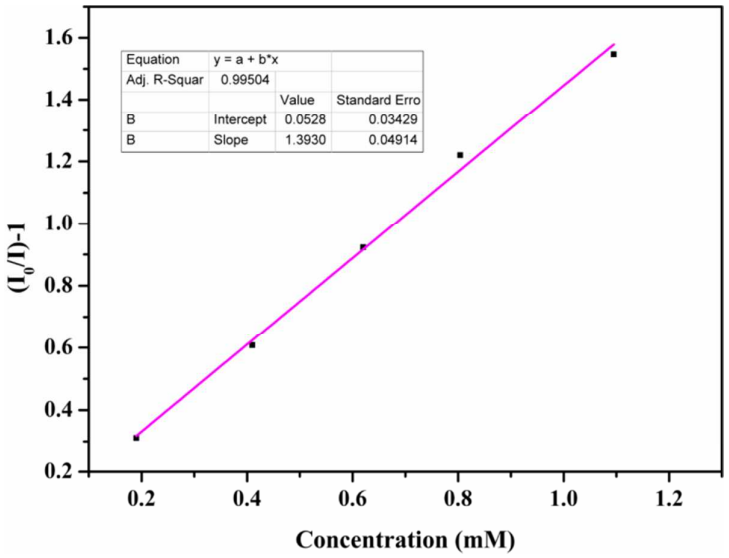

Figure S19. The Stern-Volmer plots for complex **5** with m-DNB in the low concentration region. The solid lines represent fits to the concertration-resolved data using the Stern-Volmer equation.

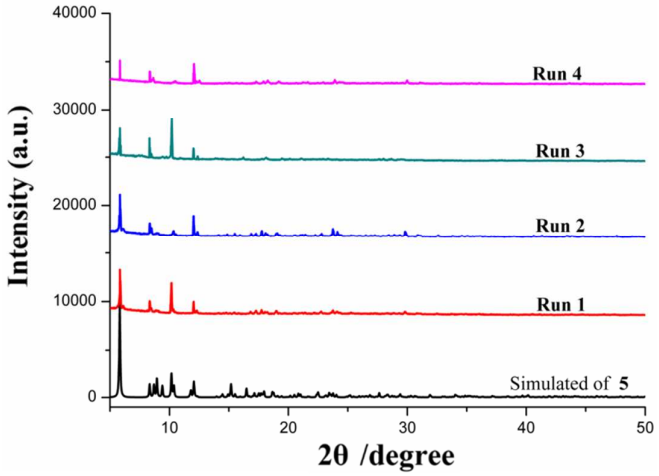

Figure S120. PXRD patterns of complex**5** after detection of TNP in DMACfor four cycles.

Table S1. Standard Deviation (σ) calculation for the detection of TNP for complex **5**.

Test	Fluorescence intensity (nm)
1	1760.06
2	1769.17
3	1753.79
4	1758.47
5	1764.55
Averagr	1761.21
Standard Deviation (σ)	5.57

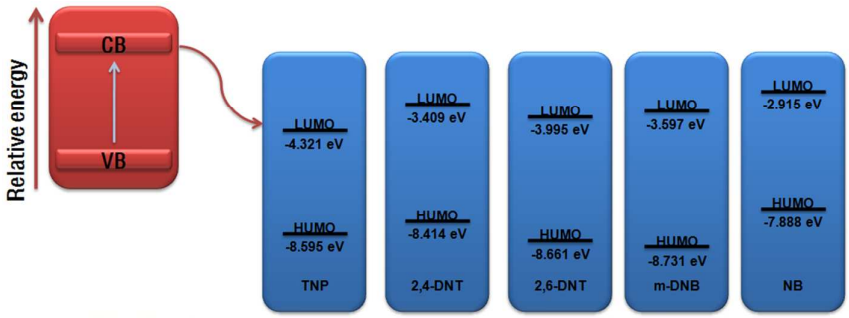

Figure S21. Schematic illustration of electron transfer process between complex **5** and NACs

Table S2. HOMO and LUMO energies of some nitro aromatic compounds. [1]

Analytes	HOMO (ev)	LUMO (ev)	Band Gap (ev)
TNP	-8.595	-4.321	4.274
2,6-DNP	-8.661	-3.995	4.666
2,4-DNP	-8.414	-3.409	5.005
NB	-8.731	-3.597	5.134
m-DNB	-7.888	-2.915	4.973

Table S3. Selected K_{sv} for TNP for complex **5** and other materials.[2-7]

Material	**Detection**	**K_{sv} (M^{-1})**	**Ref.**
UiO-67@N	TNP	2.9×10^4	2
Zn-POA	TNP	4.5×10^4	3
$[Cd(NDC)_{0.5}(PCA)]$	TNP	3.5×10^4	4
JUC-135	TNP	3.7×10^4	5
Tb(1,3,5-BTC)	TNP	3.42×10^4	6
$[Eu_3(bpybd)_3(HCOO)(\mu_3\text{-}OH)_2(H_2O)]$	TNP	2.1×10^4	7
Complex **5**	TNP	3.58×10^4	This work

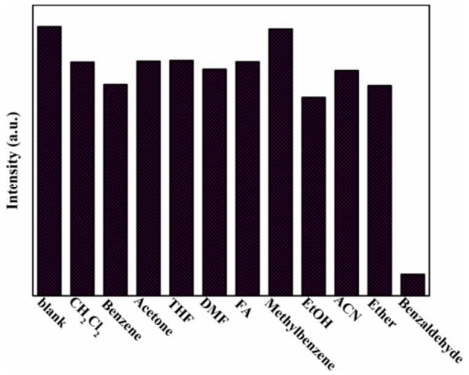

Figure S22. The lminescent intensities ($^4F_{3/2}\rightarrow{}^4F_{11/2}$) of complex **3** in suspensionexcited at 370 nmaffected by various solvents.

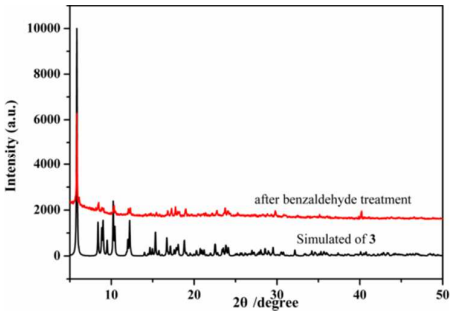

Figure S23. PXRD spectrum of the complex **3** before and after benzaldehyde treatment

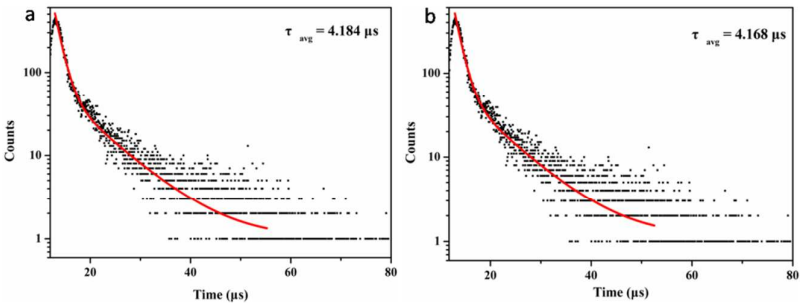

Figure S24. Room-temperature luminescence decay curves for complex **3** in the absence (a) and presence (b) of benzaldehyde (DMAC, 10 mM, 20 μL and λ_{ex} = 370 nm).

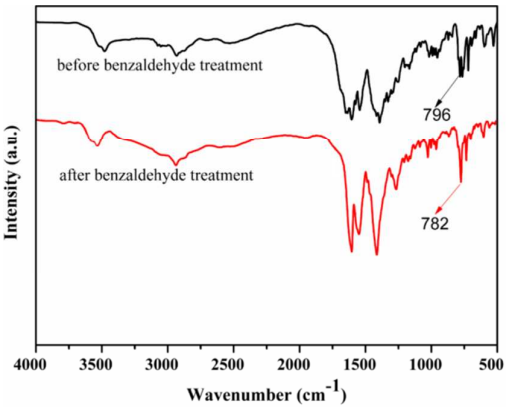

Figure S25. FT-IR spectra of Complex **3** before and after treatment with benzaldehyde

Reference:

(1) Hu, Z.; Deibert, B. J.; Li, J. *Chem. Soc. rev.* **2014,** 43, 5815-40.

(2) Nagarkar, S. S.; Desai, A. V. and Ghosh, S. K. *Chem. Commun*. **2014**, 50, 8915–8918.

(3) Jiang, X.; Liu, Y.; Wu, P.; Wang, L.; Wang, Q.; Zhu, G.; Li, X. L. *RSC. Adv.* **2014,** 4, 47357-47360.

(4) Nagarkar, S. S.; Joarder, B.; Chaudhari, A. K.; Mukherjee, S. and Ghosh, S. K. *Angew. Chem., Int. Ed*. **2013**,52, 2881–2885.

(5) He, H. M.; Song, Y.; Sun, F. X.; Bian, Z.; Gao, L. X. and Zhu, G. S. *J. Mater. Chem. A* **2015**, 3, 16598-16603.

(6) Xiao,J. D.; Qiu,L. G.; Ke,F.; Yuan,Y. P.; Xu,G. S.; Wang, Y. M. and Jiang, X. *J. Mater. Chem. A* **2013**, 1, 8745–8752.

(7) Song, X.Z.; Song, S.Y.; Zhao, S.N.; Hao, Z.M.; Zhu, M.; Meng, X.; Wu, L.L. and Zhang, H. J., *Adv. Funct. Mater.* **2014,** 24, 4034-4041.